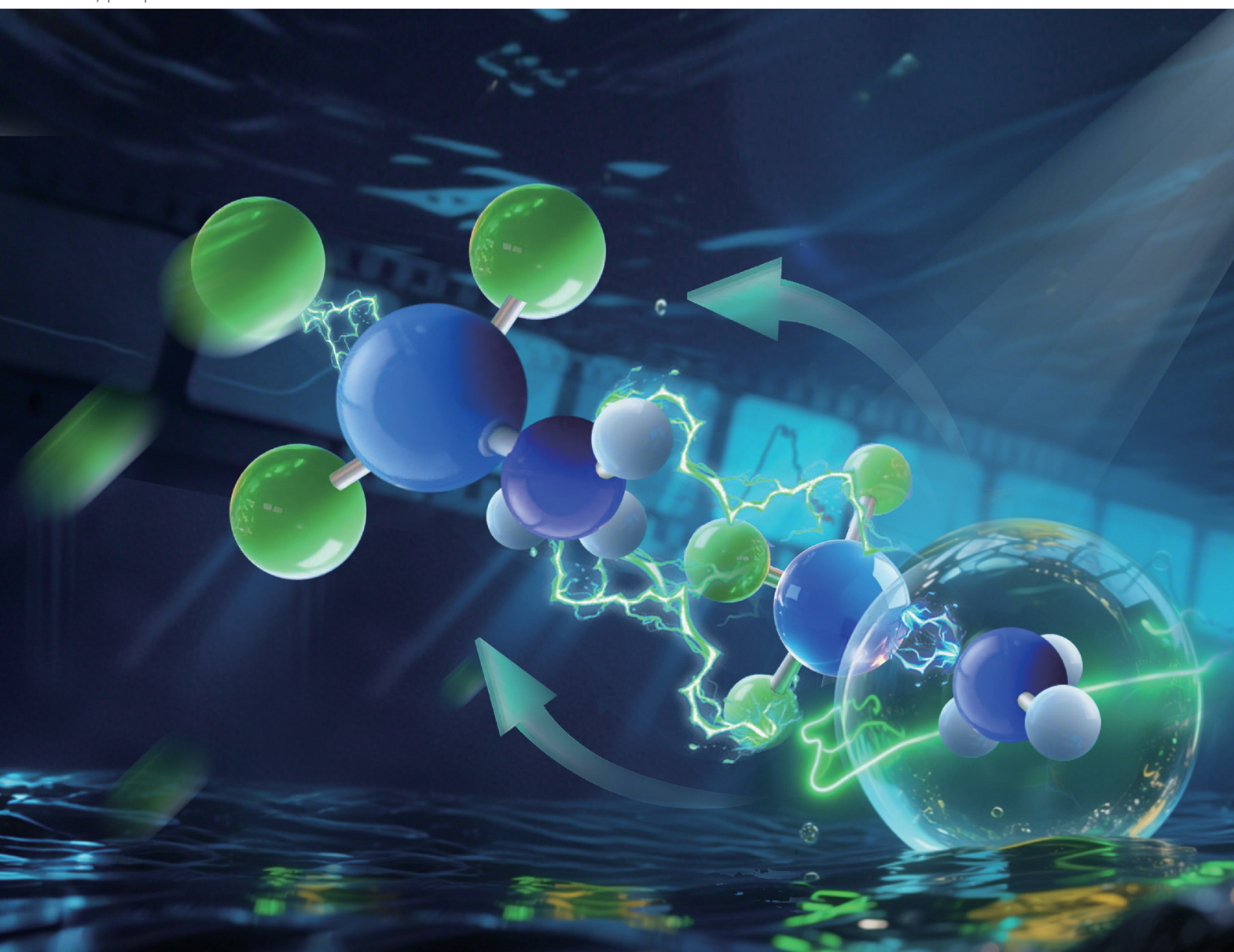
Volume 27 Number 24 28 June 2025 Pages 12605-13196

PCCP

Physical Chemistry Chemical Physics

rsc.li/pccp





ISSN 1463-9076



PAPER

Xue-Bin Wang, Zhenrong Sun, Yan Yang et al. Exploring the trans effect of the NH_3 ligand in platinum halide complexes $Pt(NH_3)ClX_2^-$ (X = Cl, Br, I) using cryogenic photoelectron spectroscopy and quantum chemical calculations



PCCP



PAPER

View Article Online



Cite this: Phys. Chem. Chem. Phys., 2025, 27, 12657

Exploring the trans effect of the NH₃ ligand in platinum halide complexes $Pt(NH_3)ClX_2^-$ (X = Cl, Br, I) using cryogenic photoelectron spectroscopy and quantum chemical calculations†

Qixu Zhao, (1) ‡a Jian Zhang, ‡b Xueying Li, a Peng Tang, a Fan Yang, a Junyang Ma, a Zhubin Hu,^a Haitao Sun, Da Xue-Bin Wang, Da Xuenrong Sun Ad and Yan Yang (1)*a

Cryogenic anion photoelectron spectroscopy, combined with quantum chemical calculations, was employed to investigate $PtClX_2^-$, $Pt(NH_3)ClX_2^-$ (X = Cl, Br, I), and their isomers. Photoelectron spectra recorded at 193 nm, supported by B3LYP-D3(BJ)/aug-cc-pVTZ(-pp) calculations, provided adiabatic (ADEs) and vertical detachment energies (VDEs) with excellent agreement between experimental and theoretical results. Coordination of the NH_3 ligand to $PtClX_2$ reduced the electron binding energy, and substantially elongated trans Pt-halogen bonds. Further computational analyses, including natural population analysis (NPA), frontier molecular orbital (FMO) studies, and dissociation energy calculations, all revealed significant changes in charge distributions and stability of trans halogen ligands. The results demonstrated that NH3 coordination notably elevated FMO orbital energies, with the extent of this elevation correlating strongly with the trans halogen's orbital contributions. These findings provide new insights into ligand-induced electronic and structural transformation in platinum halide systems and establish a theoretical foundation for understanding the underlying molecular mechanisms that dictate the activities of platinum-based anticancer drugs.

Received 1st March 2025 Accepted 1st May 2025

DOI: 10.1039/d5cp00807g

rsc.li/pccp

Introduction

The concept of the 'trans effect' was first introduced by Chernyaev in 1926 during his study of Pt(II) square planar complexes, where he observed that coordinated groups in the trans

position influence each other within a complex. Today, the trans effect is a well-established phenomenon in ligand substitution reactions of square planar and octahedral transition metal complexes. 1-3 It is defined as the influence of a coordinated group on the substitution rate of the ligand trans to itself, affecting the bond length and stability of the *trans* ligand. This phenomenon has found wide applications in fields such as medicinal chemistry and catalysis. For instance, the trans effect plays a pivotal role in the mechanisms of platinum-based anticancer drugs (e.g., cisplatin and oxaliplatin) $^{4-6}$ and catalytic processes, such as electrocatalytic CO2 reduction using Rubased catalysts.^{7,8} In the case of platinum-based anticancer drugs, where the trans effect governs ligand substitution during interaction with DNA bases, the cis-configuration ensures that the opposite ligands of leaving groups are nitrogen-containing groups, such as NH3. The NH3 ligand exerts the trans effect, facilitates ligand dissociation and enhances the drug's activity.

A substantial body of research has been conducted on platinum halide complexes with various types of ligands, such as the Zeise's salt⁹ anions $[PtX_3(C_2H_4)]^-$ (X = Cl, Br, I), among others. Utilizing high-resolution anion photoelectron spectroscopy combined with quantum chemical calculations, Hou et al.10,11 found that both the electron binding energy and the

^a State Key Laboratory of Precision Spectroscopy, and School of Physics and Electron Sciences, East China Normal University, Shanghai 200241, China. E-mail: yyang@lps.ecnu.edu.cn

^b College of Chemistry&Chemical Engineering, Donghua University, Shanghai 201620. China

^c Physical Sciences Division. Pacific Northwest National Laboratory. Richland. WA 99352, USA. E-mail: xuebin.wang@pnnl.gov

^d Collaborative Innovation Center of Extreme Optics, Shanxi University, Taiyuan, Shanxi 030006, China. E-mail: zrsun@phy.ecnu.edu.cn

[†] Electronic supplementary information (ESI) available: Initial geometries and optimized geometries of PtClX2-, Pt(NH3)ClX2- (X = Cl, Br, I) anions and the corresponding neutrals; lowest energy structures of PtClX2, Pt(NH3)ClX2 (X = Cl, Br, I), and their isomers; the HOMO energy difference upon NH3 coordination and orbital rearrangement between PtClX₂⁻ and Pt(NH₃)ClX₂⁻ (X = Br, I) anions; the LUMO plot of Pt(NH₃)Cl₃⁻; the ionic proportion of the chemical bonds Pt-Cl, Pt-Br, and Pt-I of $PtClX_2^-$, $Pt(NH_3)ClX_2^-$ (X = Cl, Br, I); the dissociation energies of different dissociation channels of PtClX2-, Pt(NH3)ClX2- and Pt(C2H4)ClX2-(X = Cl, Br, I); and the structures and bonding energies of $Pt(C_2H_4)ClX_2^-$ (X = Cl, Br. I). See DOI: https://doi.org/10.1039/d5cp00807g

[‡] These two authors contributed equally to this work.

interaction energy between the C2H4 ligand and the platinum halide decrease as the halide size increases. They also demonstrated how variations in ligand type influence the evolution of the electronic structure and molecular configuration in Zeise's family complexes. A wealth of research reporting on the physical and chemical properties of platinum halide complexes containing NH3 ligands has also been well documented. For example, Zhang et al. 12,13 focused on the vibrational properties of the NH₃ ligand in cisplantin. Warneke and Rohdenburg et al. 14,15 reported the electron-induced decomposition of cisplatin, demonstrating the NH₃ ligand's role as a reducing agent to promote Cl dissociation. Pinter et al. 16 studied the trans effect in ammine substitution reactions of trans-TPtCl₂NH₃ (T = NH₃, PH₃, CO, and C₂H₄) using energy decomposition and chemical valence analyses. Despite these efforts, the comprehensive impact of the NH₃ ligand's trans effect on the molecular configuration, electronic structure, and stability of halogenated platinum complexes has remained insufficiently explored to date. In addition, gas-phase photoelectron spectroscopy (PES) studies on halogenated platinum anions containing NH3 ligands are notably lacking.

In this work, we employ cryogenic anion cluster photoelectron spectroscopy (CRACPES) and quantum chemical calculations to systematically investigate PtClX2 (X = Cl, Br, I), $Pt(NH_3)ClX_2^-$ (X = Cl, Br, I), and their isomers. These anions provide an ideal model to explore the microscopic effects of the NH₃ ligand's trans effect in platinum halide anion complexes. The use of CRACPES enables precise measurements of electronic structures, stabilities, and energetics in the gas phase. The target anions, which cannot be prepared by electrospray ionization (ESI†) source directly, are produced through collisioninduced dissociation (CID) in a two-stage ion funnel system.

Our results demonstrate that NH₃, as an electron-donating ligand, upon binding to PtClX2-, significantly decreases the electron binding energy (eBE) and elongates the bond lengths between the halogen ligands and the platinum atom, particularly for the trans halogens. Furthermore, natural population analysis (NPA) and frontier molecular orbital (FMO) calculations reveal that the NH3 ligand transports a substantial amount of its electron density along the NH₃-Pt-trans-halogen axis and weakens the stability of the trans halogen ligands while elevating FMO energy levels. These findings provide critical insights into the fundamental role of the NH3 ligand in platinum-based anticancer drugs and offer molecular-level guidance for the design of new metal-ligand anticancer therapeutics.

Methods

CRACPES experiments

The experiments were conducted using the CRACPES system, which has been described in detail elsewhere. 17,18 KPt(NH₃)Cl₃ (Shanghai Boer Chemical Reagents) was dissolved in a water/ acetonitrile (CH₃CN) mixed solvent (1:4) to prepare a 2 mM sample solution. To generate $Pt(NH_3)ClX_2^-$ (X = Br, I), potassium halides (KBr and KI) were added to aliquots of this solution, facilitating ligand substitution reactions. PtClX2

(X = Cl, Br, I) anions were subsequently prepared via collision-induced dissociation (CID) of parent Pt(NH3)ClX2-(X = Cl, Br, I) anions. The target anions were cooled to 13 K in a two-stage linear ion trap before extraction into a TOF mass spectrometer for mass analysis. Each target anion was massselected, collimated, and momentum decelerated before being irradiated with 193 nm laser pulses (ExciStar™ XS 500, Coherent) in the interaction zone. Photodetached electrons were collected using a magnetic-bottle photoelectron spectrometer. The acquired original photoelectron TOF spectra were converted to electron kinetic energy (eKE) spectra and calibrated by the known spectra of I⁻, ¹⁹ and MnO₄⁻. ²⁰ The final electron binding energy (eBE) spectra were obtained by subtracting the eKE spectra from the detachment photon energy, with an electron energy resolution ($\Delta E/E$) of ~1.9% (i.e., ~30 meV for 1.6 eV KE electrons).

Computational methods

The structures of target anions and their corresponding neutral species were optimized using density functional theory (DFT) with the hybrid B3LYP-D3(BJ) exchange-correlation functional,²¹ which has been widely used in studying Pt-containing complexes with sufficient accuracy.22-24 The aug-cc-pVTZ-pp basis set with an effective core potential (ECP) was used for both Pt and I atoms to account for scalar relativistic effects, 25,26 while the aug-cc-pVTZ basis set was used for H, N, Cl, and Br atoms.^{27,28} Various initial structures with different spin multiplicities for both anionic and neutral species were explored to identify global minima. Vibrational frequency calculations confirmed the absence of imaginary frequencies, ensuring that the optimized structures correspond to true minima. The adiabatic detachment energy (ADE) values were determined as the energy difference between the neutral and anionic species at their respective optimized geometries, including zero-point energy (ZPE) corrections. The vertical detachment energy (VDE) values were calculated as the energy difference between the neutral and anionic species, with the neutral geometry constrained to that of the optimized anion. Excited states of the neutral species were computed using timedependent DFT (TDDFT)²⁹ at the CAM-B3LYP³⁰/aug-cc-pVTZ(-pp) level of theory. Spin-orbit coupling effects were not considered in these calculations, as these do not qualitatively impact experimental data interpretation. 31-33 Since the three-coordinated platinum halide anions exhibit a pronounced trans effect upon NH₃ ligand coordination, we employed extended transition statenatural orbitals for chemical valence (ETS-NOCV),34 natural population analysis (NPA), and ionic bonding contributions to investigate how trans effects influence charge redistribution and electronic interactions/transfer. Additionally, dissociation energy and binding energy calculations were performed to assess how the trans effect affects ligand stability at different coordination sites. For Pt(NH3)ClX2- and their isomers, ETS-NOCV analyses were performed using the Multiwfn 3.8 (dev) program.³⁵ In this approach, anions were divided into two fragments: the halogenated platinum anion and the NH3 ligand, enabling a direct examination of how NH₃ impacts the electronic distribution of the halogenated platinum moiety. Additionally, NPA charge distributions and dissociation energies were calculated at the

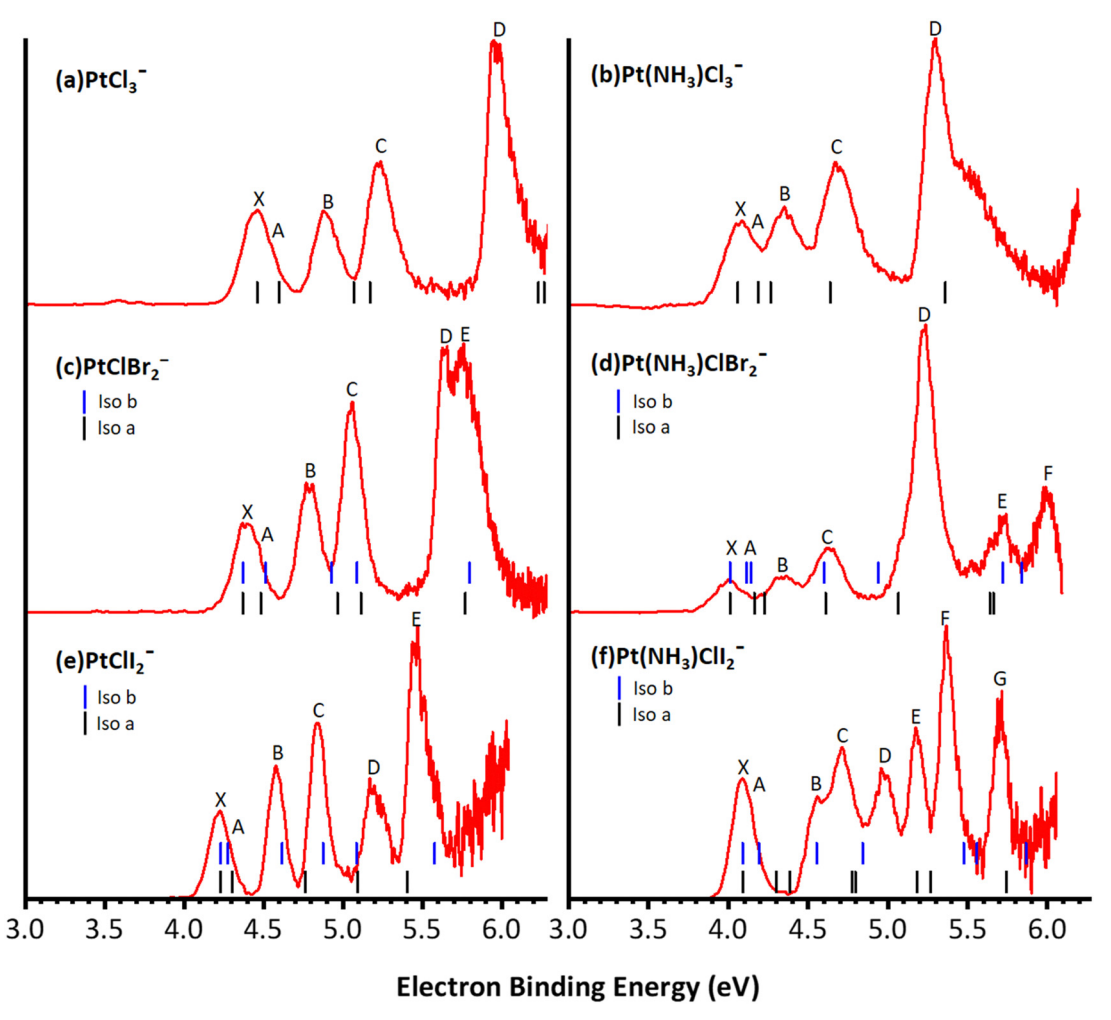
B3LYP-D3(BJ)/aug-cc-pVTZ(-pp) level of theory. The binding energies were calculated with corrections for basis set superposition error (BSSE) using the counterpoise method, and zero-point energy (ZPE) corrections derived from vibrational frequency calculations at the B3LYP-D3(BJ)/aug-cc-pVTZ(-pp) level of theory. The ionic contributions of chemical bonds were evaluated using localized molecular orbital methods implemented in the Multiwfn 3.8 (dev) program, and the highest occupied molecular orbitals (HOMOs) and the ETS-NOCV results were visualized using the VMD³⁶ program. All quantum chemical calculations were performed using the Gaussian 16 Rev. C.02,37 and Gauss-View 6 was used for structure visualization.

Results and discussion

Photoelectron spectra of target anions

Fig. 1 presents the cryogenic anion photoelectron spectra of $PtClX_2^-$ (X = Cl, Br, I) and $Pt(NH_3)ClX_2^-$ (X = Cl, Br, I) recorded

under 193 nm laser excitation. The observed spectral features, labelled as X and A-G, correspond to the transitions from the anionic ground state to the neutral ground and excited states upon electron detachment. The VDE is defined as the maximum of the X state in each spectrum, while the ADE is determined by the intersection of the tangent to the rising edge of the X state with the eBE axis, corrected for the instrumental resolution. Based on the experimental data, the ADEs values for PtClX₂ and $Pt(NH_3)ClX_2^-$ (X = Cl, Br, I) were determined to be 4.26, 4.23, 4.08, 3.85, 3.79, and 3.96 eV, respectively, while the corresponding VDE values were found to be 4.46, 4.37, 4.23, 4.06, 4.01, and 4.09 eV. Fig. 1 reveals that the coordination of an NH₃ ligand to the three-coordinate platinum halide anions results in a notable decrease in the electron binding energy, shifting the overall spectra toward lower eBE values. Additionally, while the spectral features of PtCl₃ and Pt(NH₃)Cl₃ remain largely unchanged, the spectra of $Pt(NH_3)ClX_2^-$ (X = Br, I) exhibit noticeable changes compared to those of PtClX₂⁻ (X = Br, I) in the context of spectral broadening and splitting. Notably, in the



 $\textbf{Fig. 1} \quad \text{The 193 nm cryogenic photoelectron spectra of (a) } PtCl_3^-, (b) \\ Pt(NH_3)Cl_3^-, (c) \\ PtClBr_2^-, (d) \\ Pt(NH_3)ClBr_2^-, (e) \\ PtCll_2^-, and (f) \\ Pt(NH_3)Cll_2^-. \\ \text{Vertical properties of (a) } PtCll_2^-, (b) \\ PtCll_2^$ bars indicate the energies of the ground and excited states of neutral species, calculated using TDDFT at the CAM-B3LYP/aug-cc-pVTZ(-pp) level of theory. In (c)-(f), black and blue bars represent the transition energies derived from different isomers. The calculated first VDE is shifted to align with the experimental X peak in each spectrum.

spectrum of PtClBr₂⁻, the D and E peaks appear to originate from the splitting of a single spectral feature, arising presumably from the copresence of two isomers with distinct halogen coordination geometries in the experiments. This hypothesis will be further examined through theoretical calculations in subsequent sections.

Optimized structures, calculated ADEs and VDEs

The DFT optimized, lowest-energy structures of PtClX₂⁻ and $Pt(NH_3)ClX_2^-$ (X = Cl, Br, I), are summarized in Table 1 (see Fig. S1-S3, ESI† for the details about how to construct the initial structures with different spin multiplicities, and the corresponding optimized neutral molecules). The most stable structures in Table 1 all feature a singlet electronic state with an overall similar platinum trihalide framework, in which one halide at the apex (X_a) is distinct from the other two at the base (X_b, X_b) that forms a large obtuse X_b -Pt- X_b angle (>160°). PtCl₃ has two identical Pt-Cl_b bonds of 2.310 Å, and a slightly shorter Pt-Cl_a bond at 2.247 Å. Upon coordination of NH₃ to PtCl₃⁻ from the base, trans- to the apical Cl, all Pt-Cl bonds elongate, with the elongation of the apical Cl nearly twice bigger than the base Cl (0.071 vs. 0.042 Å), while the Cl_b-Pt-Cl_b' angle increases from 166° to 172°. For PtClBr₂⁻, two low-lying isomers are identified

with the one featuring Cl at the apex (iso a) being slightly less stable by 0.07 eV compared to the other with the Br on the apical position (iso b). Attaching one NH3 molecule from the base, transpositioned to the apical halide in PtClBr₂⁻ results in two corresponding isomers of Pt(NH₃)ClBr₂⁻, in which the coordination of NH₃ induces similar geometric changes for the PtClBr₂ moiety as described in the PtCl₃ case above, i.e., substantially more elongation for the Pt-X_a bond than Pt-X_b with increased X_b-Pt-X_b' bond angles. Notably, binding NH₃ to PtClBr₂⁻ reverses the relative stability of the two isomers of PtClBr₂ with the iso a of Pt(NH₃)ClBr₂⁻ featuring a trans-Cl becoming more stable. Similarly, two isomers of PtClI₂⁻ are located with iso a featuring an apical Cl lying 0.2 eV higher in energy than iso b. Attaching one NH₃ molecule from the base of PtClI₂⁻ largely eliminates this relative energy difference and again reverses the energy order with iso a of the ammonium complex become the most stable one, but only by 0.05 eV (Table 1). The same geometric changes brought by NH₃ are observed in Pt(NH₃)ClI₂ as well.

Examining the aforementioned optimized structures evidences that the coordination of the NH₃ ligand to platinum trihalides leads to an overall elongation of the Pt-halogen bonds. Notably, the bond length of the Pt-X_a, positioned trans to NH₃, increases more significantly, showing a clear trans

Table 1 Lowest-energy structures of $PtClX_2^-$ and $Pt(NH_3)ClX_2^-$ (X = Cl, Br, I) anions optimized at the B3LYP-D3(BJ)/aug-cc-pVTZ-(pp) level of theory. The relative energy ΔE^a (in eV), bond length (in Å) and bond angles (in degree) are provided

Anions	PtClX ₂ ⁻ (singlet)		$Pt(NH_3)ClX_2^-$ (singlet)	Pt(NH ₃)ClX ₂ ⁻ (singlet)	
	Cl _b	Cl _a Pt Cl _b '	Clb	Pt Cl _b '	
$\begin{array}{l} \text{Pt-Cl}_{a} \\ \text{Pt-Cl}_{b} \\ \text{Pt-Cl}_{b'} \\ \angle \text{Cl}_{a}\text{-Pt-Cl}_{b} \\ \angle \text{Cl}_{b}\text{-Pt-Cl}_{b'} \end{array}$	2.247 2.310 2.310 97 166 Iso a $(\Delta E = 0.07)$ Cl_a Br_b Pt Br_b'	Iso b $(\Delta E = 0)$ Br_a $Cl_b Pt Br_b'$	2.318 2.352 2.352 94 172 Iso a $(\Delta E = 0)$ Cl_a Pt Br_b'	Iso b ($\Delta E = 0.03$) Br _a Cl _b Pt Br _b '	
$\begin{array}{l} \text{Pt-Cl}_{a/b} \\ \text{Pt-Br}_{a/b} \\ \text{Pt-Br}_{b'} \\ \angle \text{ Br}_{a/b} \text{-Pt-Cl}_{a/b} \\ \angle \text{ Br}_{a/b} \text{-Pt-Br}_{b'} \end{array}$	C_{2V} 2.248 2.439 2.439 98 165 Iso a $(\Delta E = 0.2)$	C_{s} 2.310 2.377 2.434 97 97 Iso b $(\Delta E = 0)$	NH ₃ 2.317 2.487 2.487 2.487 94 172 Iso a $(\Delta E = 0)$ Cl _a	2.357 2.451 2.480 94 95 Iso b $(\Delta E = 0.05)$	
$\begin{array}{l} \text{Pt-Cl}_{a/b} \\ \text{Pt-I}_{a/b} \\ \text{Pt-I}_{b}' \\ \angle \text{I}_{a/b} \text{-Pt-Cl}_{a/b} \\ \angle \text{I}_{a/b} \text{-Pt-I}_{b}' \end{array}$	2.251 2.610 2.610 98 164	Cl _b Pt l _b ' C _s 2.315 2.548 2.595 97 97	2.317 2.666 2.668 94 172	2.367 2.625 2.647 94	

 $^{^{}a}$ ΔE represents the energy difference between the isomer structure and the lowest-energy structure.

Table 2 The experimental and calculated ADEs and VDEs of PtClX₂⁻ and $Pt(NH_3)ClX_2^-$ (X = Cl, Br, I) anions. The calculations were performed at the B3LYP-D3(BJ)/aug-cc-pVTZ-(pp) level of theory

	ADE (eV)		VDE (eV)	VDE (eV)	
Anions	$\mathrm{Exp.}^a$	Calc.	$\mathrm{Exp.}^a$	Calc.	
PtCl ₃	4.26	4.18	4.46	4.35	
Pt(NH ₃)Cl ₃ ⁻	3.85	3.83	4.06	4.00	
PtClBr ₂ ⁻ (iso a)	4.23	4.13	4.37	4.28	
PtClBr ₂ (iso b)		4.12		4.26	
Pt(NH ₃)ClBr ₂ (iso a)	3.79	3.86	4.01	4.00	
Pt(NH ₃)ClBr ₂ (iso b)		3.84		3.98	
PtClI ₂ (iso a)	4.08	3.79	4.23	4.12	
PtClI ₂ (iso b)		3.99		4.10	
Pt(NH ₃)ClI ₂ (iso a)	3.96	3.80	4.09	3.90	
Pt(NH ₃)ClI ₂ (iso b)		3.77		3.86	

^a The experimental uncertainty of ADEs and VDEs is 0.02 eV.

effect, whereas the Pt-X_b bonds adjacent to the NH₃ ligand exhibit only minor changes, much less influenced by this interaction. For the mixed ligand platinum trihalides PtClX₂ (X = Br, I), iso a in which the sole Cl is at the apex is less favourable than iso b that features the apical Br or I. Binding NH₃ trans to the apex of PtClX₂ preferentially stabilizes more on iso a, rendering iso a the most stable structure for Pt(NH₃)ClX₂⁻. Additionally, Fig. S2 (ESI†) presents the optimized structure of the PtCl₃ under different spin multiplicities, showing that its D_{3h} -symmetric triplet-state structure is higher in energy by 0.29 eV, compared to its lower-symmetry singlet ground-state configuration. In addition to B3LYP-D3(BJ), we employed CAM-B3LYP and MP2 with the aug-ccpVTZ(-pp) basis set to optimize the structures of PtClX₂⁻ and $Pt(NH_3)ClX_2^-$ (X = Cl, Br, I) and compute their corresponding energies. The optimized geometries from all three methods were in close agreement. However, B3LYP-D3(BJ) provided the best match to the experimental ADE and VDE values, and its results were therefore adopted. Detailed comparisons are provided in Fig. S4 and Table S1 (ESI†).

Table 2 compares the experimental and theoretical ADE and VDE values for $PtClX_2^-$ and $Pt(NH_3)ClX_2^-$ (X = Cl, Br, I). Excluding the results of iso a of PtClI2 which is 0.2 eV less stable and unlikely contributed to the experiments, an excellent agreement between the experimental and theoretical results is found with the mean absolute errors (MAEs) of 0.096 eV for ADE and 0.106 eV for VDE. Additionally, the excited states of the neutral molecules were calculated using the anionic structures (Table 3) and compared with the corresponding spectra (see the vertical lines in Fig. 1). The simulated TDDFT stick spectra reasonably cover the observed spectral bands, but obvious deviations exist, presumably due to the lack of consideration of multi-reference nature and spin-orbit splitting effects in the calculations.

Trans effect displayed in charge distribution, MO interaction, and bonding characteristics

To further investigate the trans effect in platinum halide complexes upon NH₃ coordination, the NPA charge distributions of

Table 3 Experimentally measured and theoretically calculated VDEs and excitation energies of neutral excited states from TDDFT calculations, at the CAM-B3LYP/aug-cc-pVTZ(-pp) level. The VDE of the ground state X was calculated at the B3LYP-D3(BJ)/aug-cc-pVTZ(-pp) level

		VDEs (eV	VDEs (eV)	
Anions	States	Expt. ^c	Calc.	
PtCl ₃	X	4.46	4.35	
3	Α	4.55	4.59	
	В	4.87	5.06	
	C	5.23	5.17	
	D	5.98	6.23/6.27	
Pt(NH ₃)Cl ₃	X	4.06	4.00	
(3), 3	Α	4.16	4.19	
	В	4.35	4.26	
	C	4.67	4.64	
	D	5.30	5.35	
PtClBr ₂ ⁻ (iso a, b)	X	4.37	4.28^a . 4.26^b	
1101212 (150 a, 5)	A	4.46	4 48 ^a 4 51 ^b	
	В	4.77	$4.97^a 4.93^b$	
	C	5.05	$4.28^{a}, 4.26^{b}$ $4.48^{a}, 4.51^{b}$ $4.97^{a}, 4.93^{b}$ $5.11^{a}, 5.09^{b}$	
	D	5.63	5.80^{b}	
	E	5.75	5.77 ^a	
Pt(NH ₃)ClBr ₂ ⁻ (Iso a, b)	X	4.01	4.00 ^a , 3.98 ^b	
- 1(3)2 (,)	A	4.10	4.16^a , $4.12^b/4.14^b$	
	В	4.34	4.23	
	C	4.63	4.61^a , 4.60^b	
	D	5.23	$4.61^a, 4.60^b$ $5.07, 4.94^b$	
	E	5.72	$5.64^a/5.66^a$, 5.72^b	
	F	5.98	5.84 ^b	
PtClI ₂ ⁻ (iso a, b)	X	4.23	4.12^a , 4.10^b	
2 (*****)	Α	4.29	$4.30^a, 4.27^b$	
	В	4.58	4.76^a , 4.62^b	
	C	4.84	4.87 ^b	
	D	5.17	5.10^a , 5.09^b	
	E	5.46	$5.41^a, 5.57^b$	
Pt(NH ₃)ClI ₂ ⁻ (Iso a, b)	X	4.09	3.90^a , 3.86^b	
(- :3) = 12 (100 m, b)	A	4.14	4.30^a , 4.19^b	
	В	4.55	$3.90^{a}, 3.86^{b}$ $4.30^{a}, 4.19^{b}$ $4.39^{a}, 4.55^{b}$	
	C	4.71	$4.77^a/4.79^a$	
	D	4.96	4.84^{b}	
	E	5.18	5.18^a	
	F	5.36	5.27^a $5.48^b/5.55^b$	
	G	5.71	5.27^a , $5.48^b/5.55^b$ 5.74^a , 5.86^b	
	G	3./1	3.74 , 3.00	

^a The isomer a of $PtClX_2^-$, or $Pt(NH_3)ClX_2^-$ (X = Br, I). ^b The isomer b of $PtClX_2^-$, or $Pt(NH_3)ClX_2^-$ (X = Br, I). ^c The experimental uncertainty of VDEs is 0.02 eV.

the corresponding anions were examined (Fig. 2). In PtCl₃⁻, the central Pt atom carries a positive charge of 0.23, while the apical Cl is at -0.29 and two other Cl ligands at the base possess more negative charges of -0.47. This trend of NPA charges among three Cl atoms can be attributed to that the apical Cl ligand is adjacent to two negatively charged Cl atoms, affording a maximum reduction in electrostatic repulsion. Substituting two base Cl ligands in PtCl₃⁻ by two Br or two I generate iso a of PtClBr₂⁻ or PtClI₂, respectively, with a structure similar to that of PtCl₃. The amount of negative charges of the base halogens follow their electron negativity, in the order of Cl > Br > I, accompanied by a gradual reduction of the Pt positive charge. Notably, the charge at the apical Cl atom remains largely unchanged and is significantly lower than those at the base ligands. In iso b of PtClBr₂⁻/PtClI₂⁻,

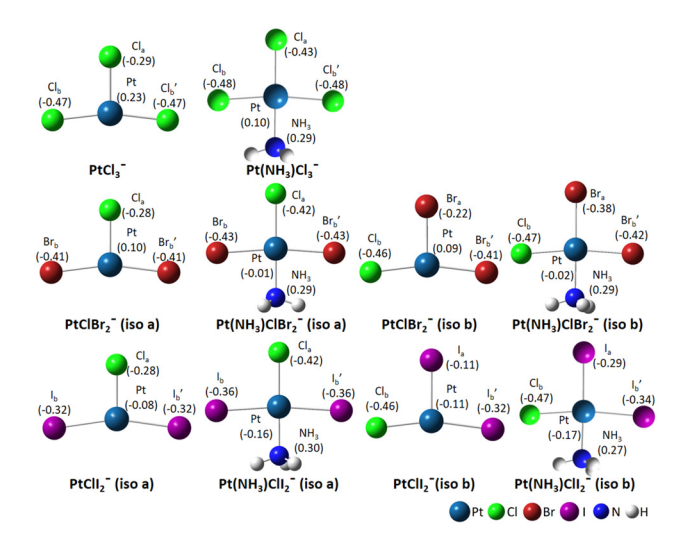


Fig. 2 The natural population analysis (NPA) charge distribution of $PtClX_2^-$ and $Pt(NH_3)ClX_2^-$ (X = Cl, Br, I) anions, calculated at the B3LYP-D3(BJ)/aug-cc-pVTZ-(pp) level of theory.

the apical Br_a/I_a ligand also consistently possesses notable fewer negative charges than the other two halogens at the base. On going from PtCl₃⁻ to PtClBr₂⁻ and PtClI₂⁻, the positive charge on Pt reduces progressively, and becomes even negative in PtClI2-, following the electron affinities of halogens in the order Cl > Br > I.

Upon NH₃ coordination in Pt(NH₃)Cl₃⁻, the charges on the two base Cl atoms remain largely unchanged, while the positive charge on the central Pt atom decreases significantly. Concomitantly, the amount of negative charge on the apical Cl atom increases noticeably, and the NH₃ ligand itself carries a partial positive charge. The above NPA charge analyses suggest that NH₃, as an electron-donating group, transfers its electron density primarily to the central Pt and apical Cl atom. The induced NPA charge distribution change upon coordination of NH_3 in $Pt(NH_3)ClX_2^-$ (X = Br, I) closely resembles those observed in the Pt(NH₃)Cl₃ case. Specifically, the halogen ligand positioned trans to NH₃ exhibits a significantly increased negative charge, whereas those at the base remain nearly intact.

To visualize the impact of the trans effect on electron transfer upon NH₃ coordination, ETS-NOCV calculations were performed. The results indicate that the NH₃ coordination induces electron transfer predominately from NH₃ (blue, negative orbital density) to its opposite halogen ligand (green, positive orbital density), while the adjacent ligands remain largely unaffected (Fig. 3). This observation is consistent with the NPA charge distribution analysis, in which the negative charge on the trans halogen ligand substantially increases after NH₃ coordination, independent of the halogen type, highlighting the dominate role of the trans effect in this process. Furthermore, the trans effect induced by NH₃ coordination significantly impacts the polarity of the trans Pt-halogen bonds. As shown in Fig. 4, the ionic character of the trans Pthalogen bond increases by more than 16% after NH₃ coordination, whereas the ionic character of Pt to the adjacent halogen ligands changes less than 1.5%. Detailed data on the ionic

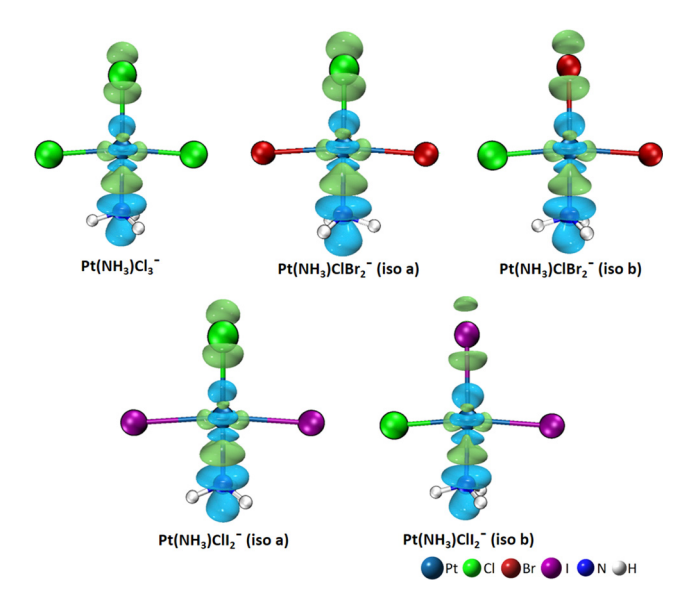


Fig. 3 The calculated ETS-NOCV of Pt(NH₃)Cl₃⁻, Pt(NH₃)ClBr₂⁻ (iso a and b) and Pt(NH₃)Cll₂ (iso a and b) with the isovalue of 0.005 at the B3LYP-D3(BJ)/aug-cc-pVTZ-(pp) level of theory. The colour green represents the positive orbital density and blue represents negative. The corresponding orbital interactions induce electron transfer from the blue region to the areen region

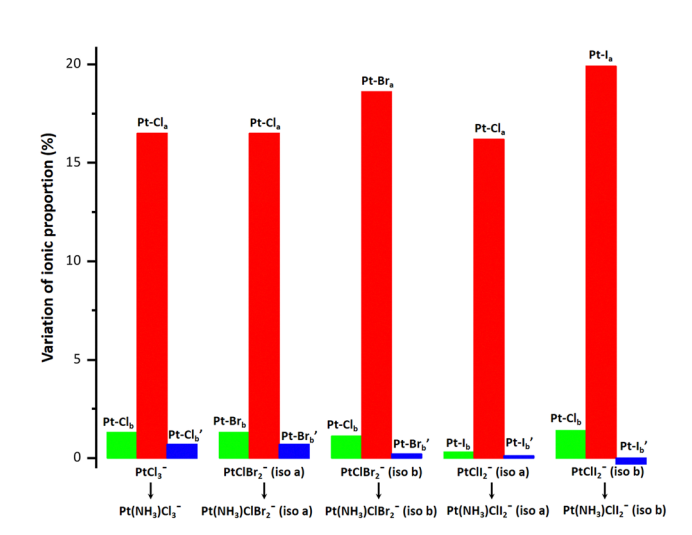


Fig. 4 The difference in ionic proportion of the corresponding Pt-halogen bonds in $PtClX_2^-$ and $Pt(NH_3)ClX_2^-$ (X = Cl, Br, I). The calculations were performed at the B3LYP-D3(BJ)/aug-cc-pVTZ-(pp) level of theory.

character are provided in Table S1 (ESI†). These results demonstrate the pronounced trans effect brought by coordinating NH3 in platinum trihalides.

Additionally, the trans effect also influences the frontier molecular orbitals (FMOs) of the system. Taking PtCl₃ and Pt(NH₃)Cl₃ as an example, NH₃ coordination does not significantly alter the orbital shapes but upshifts their energies, making them easier to ionize. Molecular orbitals with a higher contribution from the apical Cl atom in PtCl₃⁻ (HOMO-2, HOMO-4) exhibit greater energy upshifts upon the trans NH3 binding in Pt(NH₃)Cl₃⁻, which can even cause orbital reordering, i.e.,

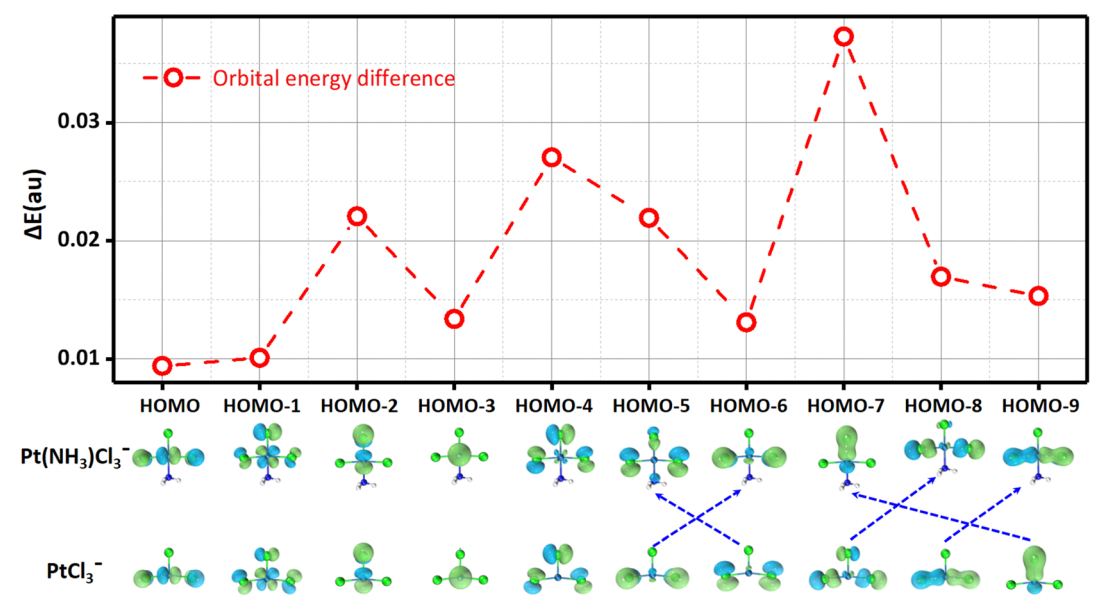


Fig. 5 The HOMO energy difference upon NH $_3$ coordination and orbital rearrangement between PtCl $_3^-$ and Pt(NH $_3$)Cl $_3^-$ with the pictures of the corresponding MOs illustrated. $\Delta E = \varepsilon$ (FMO)(PtNH₃Cl₃⁻) $- \varepsilon$ (FMO)(PtCl₃⁻) for FMO = HOMO-1, -2, -3, -4; and the correlated orbital energy differences (lined by blue lines) for deeper FMOs (HOMO-5,-6,...,-9). The calculations were performed at the B3LYP-D3(BJ)/aug-cc-pVTZ-(pp) level of theory.

HOMO-6 and HOMO-9 of PtCl₃ become HOMO-5 and HOMO-7 of Pt(NH₃)Cl₃⁻, respectively (Fig. 5). Consistent trends are observed from $PtClX_2^-$ (X = Br, I) to $Pt(NH_3)ClX_2^-$ (X = Br, I) (Fig. S5-S8, ESI†).

Previous studies have established that cisplatin (cis-Pt(NH₃)₂Cl₂) exhibits potent anticancer activity, whereas its trans analogue transplatin (trans-Pt(NH₃)₂Cl₂) is inactive. 38-40 The structural difference between the two lies in the spatial arrangement of the two NH₃ ligands: in cisplatin, each NH3 ligand is positioned trans to a Cl atom, while in transplatin, two NH3 ligands (also two Cl) face each other from the opposite side. During the drug activation process inside the cell, the Cl ligand opposite to the NH₃ ligand in cisplatin undergoes dissociation. Table 4 presents the theoretical bond dissociation energies (BDE) of Pt-Cl_a and Pt-Cl_b. In PtCl₃-, the Pt-Cl_a bond has the shortest bond length of 2.247 Å and highest BDE of 3.61 eV compared to that of Pt-Cl_b (2.310 Å, 3.29 eV). Upon NH₃ combination, the *trans* effect elongates Pt-Cl_a in Pt(NH₃)Cl₃⁻ to 2.318 Å and substantially weakens this bond with BDE = 2.90 eV, rendering it the weakest bond prone to dissociate. More BDE calculations in PtClX₂⁻ and Pt(NH₃)ClX₂⁻ (X = Br, I) (Table S2, ESI†) reveal the same trend, further corroborating the significant role of the trans effect in facilitating the trans halide dissociation by binding a NH₃ ligand.

Based on these findings, we speculate that in cisplatin and other cis-structured metal-based anticancer drugs, the leaving group ligands are those positioned opposite to the NH₃ ligand. In contrast, transplatin has halide ligands all at the adjacent, not trans position to NH₃, rendering them less susceptible to this effect. Although the drug activation mechanism occurs in vivo and under liquid-phase environments, our gas-phase study provides valuable insights into the underlying molecular mechanisms that govern such metal-based anticancer drug activities and offers benchmark references for future research aimed at designing therapeutic agents with greater efficacy.

To further investigate the trans effect in tetracoordinated platinum halide complexes with different ligands, we optimized the structures of Zeise's salt analogs, $Pt(C_2H_4)ClX_2^-$ (X = Cl, Br, I), using the same level of theory (B3LYP-D3(BJ)/aug-cc-pVTZ(-pp)) (Table S4, ESI†). Structural comparisons between PtClX₂⁻ and Pt(C₂H₄)ClX₂⁻ reveal a pronounced trans effect induced by ethylene coordination, characterized by a significant elongation of the Pt-X bond trans to the C₂H₄ ligand. Taking Pt(NH₃)Cl₃⁻ and Pt(C₂H₄)Cl₃ as representative examples, we compared their structural parameters and ligand dissociation energies. Upon coordination, the Pt-Cl_a bond trans to NH₃ elongates to 2.318 Å with a corresponding dissociation energy of 2.90 eV. In contrast, in Pt(C₂H₄)Cl₃⁻, the trans Pt-Cl_a bond elongates further to 2.338 Å, with a slightly lower dissociation energy of 2.82 eV (Table S5, ESI†). These observations demonstrate that the trans effect exerted by C₂H₄ is more pronounced than that of NH₃, as

Table 4 The dissociation energies of different dissociation channels of PtCl₃⁻ and Pt(NH₃)Cl₃⁻. All calculations were carried out at the B3LYP-D3(BJ)/ aug-cc-pVTZ-(pp) level of theory

Channel no.	Dissociation channels	E (eV)	Dissociation channels	E (eV)
1	$\begin{array}{ccc} \operatorname{PtCl}_{3}^{-} & \to \operatorname{PtCl}_{2} + \operatorname{Cl}_{a}^{-} \\ \operatorname{PtCl}_{3}^{-} & \to \operatorname{PtCl}_{2} + \operatorname{Cl}_{b}^{-} \\ \operatorname{PtCl}_{3}^{-} & \to \operatorname{PtCl}_{2} + \operatorname{Cl}_{b}^{\prime} \end{array}$	3.61	$Pt(NH_3)Cl_3^- \to Pt(NH_3)Cl_2 + Cl_a^-$	2.90
2		3.29	$Pt(NH_3)Cl_3^- \to Pt(NH_3)Cl_2 + Cl_b^-$	2.93
3		3.29	$Pt(NH_3)Cl_3^- \to Pt(NH_3)Cl_2 + Cl_b^{}$	2.93

reflected in both greater bond elongation and reduced bond strength for the trans-positioned halide. To further assess the coordination strength of the two ligands, we calculated the binding energies (BEs) of NH₃ and C_2H_4 with PtCl X_2 (X = Cl, Br, I), incorporating both basis set superposition error (BSSE) and zero-point energy (ZPE) corrections. The results show that the Pt-C₂H₄ interaction is consistently stronger than that of Pt-NH₃, suggesting that the C₂H₄-coordinated complexes are thermodynamically more stable. Detailed structural parameters, dissociation energies, and binding energies are provided in Tables S4-S6 (ESI†). Previous work by Hou et al.41 reported significant backdonation from the Pt center to the ethylene ligand in Zeise's salt complexes, which inspired us to investigate whether a similar interaction occurs in Pt(NH₃)Cl₃⁻. However, as shown in Fig. S9 (ESI†), an examination of the LUMO to LUMO+10 orbitals in Pt(NH₃)Cl₃⁻ reveals no evidence of back-donation from Pt to the NH₃ ligand, further supporting its role as a classical σ -donor.

Conclusions

In this contribution, we report a combined photoelectron spectroscopic and theoretical study on PtClX2 in comparison to their corresponding NH₃ complexes Pt(NH₃)ClX₂⁻ (X = Cl, Br, I), aimed to provide a molecular level understanding on the widely accepted 'trans effect' proposed nearly 100 years ago. Our results show that introducing an electron-donating NH3 ligand leads to a decrease in the eBE of the platinum trihalide anions, and facilitates electron transfer primarily along the H₃N-Pt-X_a axis to the trans positioned halogen ligand. Furthermore, our study demonstrates that the most stable apex halide ligand undergoes a substantial reduction in BDE upon NH3 coordination, manifesting an auspicious trans effect. At the electronic state level, this research elucidates how the trans effect influences the physical and chemical properties of platinum trihalide anions when coordinated with NH₃. Finally, we also conducted a comparison with the widely utilized Zeise's salt system. The results reveal that $PtClX_2^-$ (X = Cl, Br, I) coordinated with C_2H_4 similarly exhibits a pronounced trans effect, and the influence of this effect on the stability of the trans ligand is slightly greater than that observed with the NH₃ ligand. These findings provide valuable insights into transition-metal systems and establish a theoretical foundation for understanding platinum-based anticancer drugs, aiding in their design and synthesis.

Author contributions

Qixu Zhao: investigation (equal); writing – original draft (equal); formal analysis (equal). Jian Zhang: investigation (equal); writing – original draft (equal); formal analysis (equal). Xueying Li: resources (equal); data curation (supporting). Peng Tang: resources (equal); investigation (supporting). Fan Yang: data curation (lead). Junyang Ma: visualization (equal). Zhubin Hu: software (supportingl); visualization (equal). Haitao Sun: software (lead). Xue-Bin Wang: writing – review and editing (lead); conceptualization (equal). Zhenrong Sun: writing – review and editing (equal); funding acquisition

(lead); conceptualization (equal). Yan Yang: writing – review and editing (equal); conceptualization (lead); validation (lead).

Data availability

The data supporting this article have been included as part of the ESI. \dagger

Conflicts of interest

The authors have no conflicts to disclose.

Acknowledgements

The work was partly supported by the National Natural Science Foundation of China (No. 92461301, 12034008, and 12250003) and the Program of Introducing Talents of Discipline to Universities 111 Project (B12024). X.-B. W. was supported by the US. Department of Energy (DOE), Office of Science, Office of Basic Energy Sciences, Division of Chemical Science, Geosciences, and Biosciences, Condensed Phase and Interfacial Molecular Science program, FWP 16248.

Notes and references

- 1 F. R. Hartley, Chem. Soc. Rev., 1973, 2, 163-179.
- 2 R. G. Pearson, Inorg. Chem., 1973, 12, 712-713.
- 3 B. J. Coe and S. J. Glenwright, *Coord. Chem. Rev.*, 2000, **203**, 5–80.
- 4 M. H. Baik, R. A. Friesner and S. J. Lippard, *J. Am. Chem. Soc.*, 2003, **125**, 14082–14092.
- 5 D. V. Deubel, J. Am. Chem. Soc., 2006, 128, 1654-1663.
- 6 Y. Mantri, S. J. Lippard and M. H. Baik, J. Am. Chem. Soc., 2007, 129, 5023–5030.
- 7 S. Gonell, M. D. Massey, I. P. Moseley, C. K. Schauer, J. T. Muckerman and A. J. M. Miller, *J. Am. Chem. Soc.*, 2019, **141**, 6658–6671.
- 8 S. Gonell, E. A. Assaf, K. D. Duffee, C. K. Schauer and A. J. M. Miller, *J. Am. Chem. Soc.*, 2020, 142, 8980–8999.
- W. C. Zeise and O. K. Dan, *Vidensk. Selsk. Forh.*, 1825–1826,
 13–14.
- 10 G. L. Hou, H. Wen, K. Lopata, W. J. Zheng, K. Kowalski, N. Govind, X. B. Wang and S. S. Xantheas, *Angew. Chem., Int. Ed.*, 2012, 51, 6356–6360.
- 11 G.-L. Hou, N. Govind, S. S. Xantheas and X.-B. Wang, *J. Phys. Chem. A*, 2018, **122**, 1209–1214.
- 12 A. M. Amado, S. M. Fiuza, M. P. M. Marques and L. A. E. Batista de Carvalho, J. Chem. Phys., 2007, 127, 185104.
- 13 C. Zhang, E. B. Naziga and L. Guidoni, *J. Phys. Chem. B*, 2014, **118**, 11487–11495.
- 14 J. Warneke, M. Rohdenburg, Y. Zhang, J. Orszagh, A. Vaz, I. Utke, J. T. M. De Hosson, W. F. van Dorp and P. Swiderek, J. Phys. Chem. C, 2016, 120, 4112–4120.

PCCP

- 15 M. Rohdenburg, P. Martinović, K. Ahlenhoff, S. Koch, D. Emmrich, A. Gölzhäuser and P. Swiderek, J. Phys. Chem. C, 2019, 123, 21774-21787.
- 16 B. Pinter, V. Van Speybroeck, M. Waroquier, P. Geerlings and F. De Proft, Phys. Chem. Chem. Phys., 2013, 15, 17354-17365.
- 17 P. Tang, J. Zhang, X. Li, F. Yang, Q. Zhao, J. Ma, Z. Hu, H. Sun, X.-B. Wang, Z. Sun and Y. Yang, J. Phys. Chem. A, 2024, 128, 5500-5507.
- 18 Q. Zhao, J. Zhang, X. Li, P. Tang, F. Yang, J. Ma, Z. Hu, H. Sun, X.-B. Wang, Z. Sun and Y. Yang, J. Chem. Phys., 2024, **161**, 214305.
- 19 D. Hanstorp and M. Gustafsson, J. Phys. B:At., Mol. Opt. Phys., 1992, 25, 1773.
- 20 J. Zhang, Z.-R. Sun and X.-B. Wang, J. Phys. Chem. A, 2015, 119, 6244-6251.
- 21 N. Mehta, M. Casanova-Páez and L. Goerigk, Phys. Chem. Chem. Phys., 2018, 20, 23175-23194.
- 22 J. Joseph, K. Pradhan, P. Jena, H. Wang, X. Zhang, Y. Jae Ko and K. H. Bowen, J. Chem. Phys., 2012, 136, 194305.
- 23 Y. Shi, S. Bian, Y. Ma, Y. Wang, J. Ren and X. Kong, J. Phys. Chem. A, 2018, 123, 187-193.
- 24 R. Wesendrup and P. Schwerdtfeger, Inorg. Chem., 2001, 40, 3351-3354.
- 25 K. A. Peterson, B. C. Shepler, D. Figgen and H. Stoll, J. Phys. Chem. A, 2006, 110, 13877-13883.
- 26 D. Figgen, K. A. Peterson, M. Dolg and H. Stoll, J. Chem. Phys., 2009, 130, 164108.
- 27 R. A. Kendall, T. H. Dunning, Jr. and R. J. Harrison, J. Chem. Phys., 1992, 96, 6796-6806.
- 28 D. E. Woon and T. H. Dunning, Jr., J. Chem. Phys., 1993, 98, 1358-1371.
- 29 E. Runge and E. K. U. Gross, Phys. Rev. Lett., 1984, 52,
- 30 T. Yanai, D. P. Tew and N. C. Handy, Chem. Phys. Lett., 2004, 393, 51-57.

- 31 Y. Wei, B.-W. Wang, S.-W. Hu, T.-W. Chu, L.-T. Tang, X.-Q. Liu, Y. Wang and X.-Y. Wang, J. Phys. Org. Chem., 2005, 18, 625-631.
- 32 M. Otsuka, H. Mori, H. Kikuchi and K. Takano, Comput. Theor. Chem., 2011, 973, 69-75.
- 33 J. C. Gómez Martín, O. Gálvez, M. T. Baeza-Romero, T. Ingham, J. M. C. Plane and M. A. Blitz, Phys. Chem. Chem. Phys., 2013, 15, 15612-15622.
- 34 M. P. Mitoraj, A. Michalak and T. Ziegler, J. Chem. Theory Comput., 2009, 5, 962-975.
- 35 T. Lu and F. Chen, J. Comput. Chem., 2012, 33, 580-592.
- 36 W. Humphrey, A. Dalke and K. Schulten, J. Mol. Graph., 1996, 14, 33-38.
- 37 M. J. Frisch, G. W. Trucks, H. B. Schlegel, G. E. Scuseria, M. A. Robb, J. R. Cheeseman, G. Scalmani, V. Barone, G. A. Petersson, H. Nakatsuji, X. Li, M. Caricato, A. V. Marenich, J. Bloino, B. G. Janesko, R. Gomperts, B. Mennucci, H. P. Hratchian, J. V. Ortiz, A. F. Izmaylov, J. L. Sonnenberg, D. Williams-Young, F. Ding, F. Lipparini, F. Egidi, J. Goings, B. Peng, A. Petrone, T. Henderson, D. Ranasinghe, V. G. Zakrzewski, J. Gao, N. Rega, G. Zheng, W. Liang, M. Hada, M. Ehara, K. Toyota, R. Fukuda, J. Hasegawa, M. Ishida, T. Nakajima, Y. Honda, O. Kitao, H. Nakai, T. Vreven, K. Throssell, J. A. Montgomery Jr., J. E. Peralta, F. Ogliaro, M. J. Bearpark, J. J. Heyd, E. N. Brothers, K. N. Kudin, V. N. Staroverov, T. A. Keith, R. Kobayashi, J. Normand, K. Raghavachari, A. P. Rendell, J. C. Burant, S. S. Iyengar, J. Tomasi, M. Cossi, J. M. Millam, M. Klene, C. Adamo, R. Cammi, J. W. Ochterski, R. L. Martin, K. Morokuma, O. Farkas, J. B. Foresman and D. J. Fox, Gaussian 16, Revision B.01, Gaussian, Inc., Wallingford, CT, 2016.
- 38 L. Bica, P. J. Crouch, R. Cappai and A. R. White, Mol. BioSyst., 2009, 5, 134-142.
- 39 P. Faller, ChemBioChem, 2009, 10, 2837-2845.
- 40 P. Faller and C. Hureau, Dalton Trans., 2009, 1080-1094.
- 41 T. Yang, Z. Li, X. B. Wang and G. L. Hou, Chem. Phys. Chem., 2023, 24, e202200835.